DOI 10.1007/s10946-020-09848-y
Journal of Russian Laser Research, Volume 41, Number 1, January, 2020

AUTOMATIC FOCUSING CONTROL IN BEACONLESS APT SYSTEM

Xizheng Ke[1,2] and Pu Zhang[1*]

[1] *Faculty of Automation and Information Engineering*
Xi'an University of Technology
Xi'an 710048, China

[2] *Shaanxi Civil-Military Integration Key Laboratory*
of Intelligence Collaborative Networks
Xi'an 710126, China

*Corresponding author e-mail: puzhangxaut@163.com

Abstract

The beaconless acquisition pointing and tracking (APT) system uses signal light to act as beacon. But the signal light's divergence angle is so small that it is difficult to capture. In this work, aiming at the different requirements of divergence angle for a free-space optical-communication (FSO) system in a different working phase, we use a stepper motor for automatic focusing control in the acquisition and pointing process to change the spot size. For this purpose, we derive a formula for the average acquisition time of continuous raster scanning. The relationship between the received power and the divergence angle under the influence of the atmospheric transmission and the pointing errors is analyzed to obtain the optimum range of the divergence angle. Also the relationship between defocusing and the divergence angle of collimated beam is given. Finally, we prove by experiments that the automatic focusing control method effectively solves the contradiction of the different divergence angles between communication phase and acquisition phase.

Keywords: APT, divergence angle, beaconless, acquisition.

1. Introduction

The precondition of establishing free-space optical communication (FSO) is to keep precise alignment of the optical axes of both transceivers. Due to the narrow laser-beam divergence and strong directivity, communication beams need extremely accurate pointing [1–4]. When the laser propagates in the atmosphere, it will be affected by turbulent refractive-index fluctuation, resulting in spot jitter, beam drift, and light intensity fluctuation, which will adversely affect the normal reception of optical signals, and even lead to communication interruption [5]. Consequently, the acquisition pointing and tracking (APT) system is needed to establish accurate and reliable wireless laser communication links and to compensate the disturbance caused by atmospheric turbulence.

The acquisition mode of an APT system is divided into two kinds according to the light source – one is beacon acquisition and the other is beaconless acquisition. The acquisition time is usually related to the scanning speed, divergence angle, and the size of the scanning uncertain region [6, 7]. The divergence angle of the signal light is usually only tens of microradians, the scanning step is small, and the acquisition duration is long. So the acquisition technology mostly uses beacon with large divergence angle

Manuscript submitted by the authors in English on November 4, 2019.

to capture, and then switch to signal light with small divergence angle to communicate [8,9]. However, the atmospheric refractive index is related to the beam wavelength. If the beacon wavelength and the signal wavelength used in the acquisition phase are different, the deviation between the communication link and the beacon link will occur. In addition, beacon acquisition requires additional optical components such as high-power beacon lasers and splitting prism, which increases the complexity, power consumption, and cost of the system [10]. In order to meet the requirements of integration, lightweight, and miniaturization of FSO networks, APT systems tend to study beaconless acquisition methods in recent years.

In this paper, we analyze the average acquisition time of beams with different divergence angles and the receiving power affected by atmospheric transmission and pointing errors and obtain the range of the optimum divergence angle of beams in the acquisition and communication phases. In order to improve the acquisition efficiency and communication system performance, we use a stepper motor to focus the transmitting antenna according to different requirements of the beam divergence angle in the acquisition and communication phases of the FSO system.

This paper is organized as follows.

We introduce the structure and work flow of an automatic focusing APT system in Sec. 2. In Sec. 3, we analyze the acquisition time and the relationship between the receiving power and the divergence angle of signal light under the influence of atmospheric transmission and pointing error and give the relationship between defocussing and the divergence angle. The feasibility of the automatic focusing APT system is verified by experiments in Sec. 4. In Sec. 5, we conclude with the results obtained.

2. Automatic Focusing APT System

The schematic diagram of the automatic focusing APT system is shown in Fig. 1. The capture alignment actuator is a high-precision two-dimensional pan tilt that has a dynamic range sufficient to cover the entire scanning area. The focusing actuator is a two-phase hybrid stepping motor, which adjusts the beam size in different working phase. A charge coupled-device (CCD) camera with a wide field of view (covering the whole capturing uncertain cone) is used in the receiver capture detector, so the receiver can capture the detected beam without adjusting the direction of the detector, which helps to shorten the acquisition duration. A global system for mobile-communication (GSM) module is used

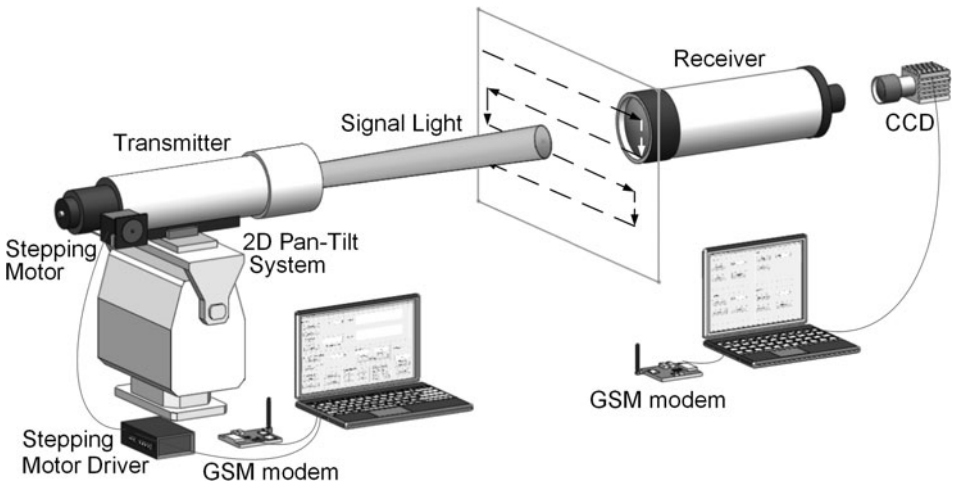

Fig. 1. Automatic focusing APT system schematic diagram.

for radio-frequency (RF) communication, which is used to realize information transmission between two terminals in the acquisition and alignment stage before establishing the communication link.

The double-ended working flow diagram of the beaconless light APT system is shown in Fig. 2.

The automatic focusing APT system works at the beginning, and the optical spacing of the transmitting antenna is adjusted by a stepping motor to increase the divergence angle of signal light. The two terminals of communication are "staring" and "scanning," respectively. The transmitter's pan-tilt-control signal light scans continuously from the starting point of scanning to the position of the receiving terminal in the uncertain cone (UC) and does not wait for the feedback instruction of the receiving terminal in the scanning process. When the spot is captured by the CCD camera, GSM sends stop instruction to the transmitting terminal. After the GSM at the transmitting terminal receives the stop instruction, the transmitting terminal stops scanning and compensates for the delay caused by radio-frequency auxiliary communication to complete the acquisition work. After the receiving terminal captures the spot, image processing is carried out to get the spot size and position information, which is used as a feedback to drive the stepper motor to adjust the divergence angle and perform pointing until the spot size and pointing errors meet the set threshold and complete the establishment of communication link.

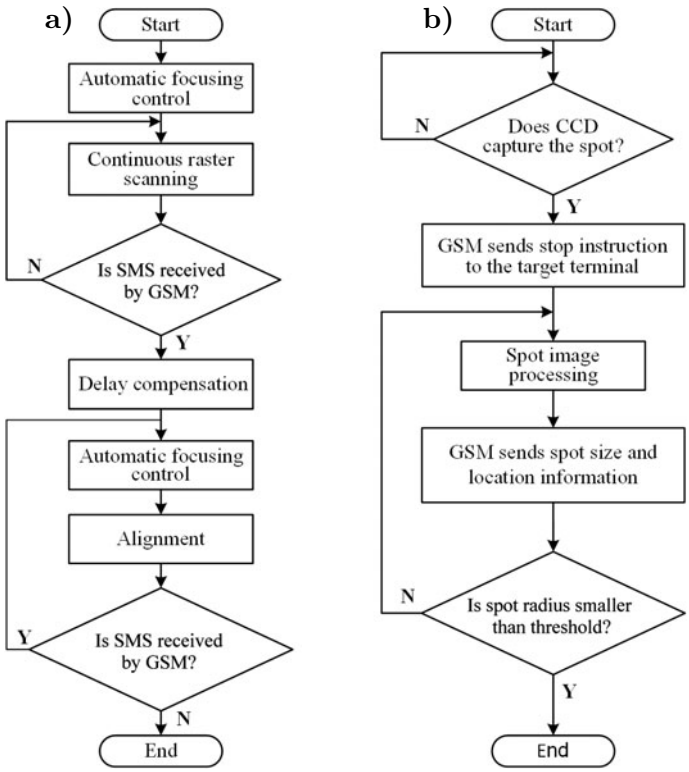

Fig. 2. Automatic focusing APT double-end workflow diagram; here, scanning end (a) and staring end (b).

3. Theoretical Model and Simulation

3.1. Average Acquisition Duration

Because of positioning error, position calculation error, and system calibration error, there are initial alignment errors between communication terminals. The angular deviation of elevation and horizontal obeys the standard normal distribution, being independent of each other. The probability density function (PDF) of radial pointing error can be described as follows [11]:

$$f(\theta_v, \theta_h) = f(\theta_v) f(\theta_h) = \frac{1}{2\pi\sigma_v\sigma_h} \exp\left[-\frac{1}{2}\left(\frac{\theta_v^2}{\sigma_v^2} + \frac{\theta_h^2}{\sigma_h^2}\right)\right], \tag{1}$$

where θ_v and θ_h represent the angular deviation of elevation and horizontal, respectively, and σ_v and σ_h are their standard deviations.

Taking the center of the scanning range as the origin, the scanning range in the elevation and horizontal directions is $\pm\theta_{uv}/2$ and $\pm\theta_{uh}/2$, the coordinates of the receiving end in the coordinate system are (θ_h,

θ_v), and the elevation and horizontal of the raster scanning can be expressed as

$$L = L_h + L_v \approx \frac{1}{2}\left[\frac{\theta_{uh} + 2\theta_h}{I_\theta}\theta_{uv} + \theta_{uv} - 2\theta_v\right]. \tag{2}$$

In Eq. (2), I_θ is the scanning interval, which is related to the divergence angle. In order to avoid the scanning gap between scanning paths, there is a certain overlapping area in the two near scanning fields expressed by the overlap factor K, which is usually 10% – 15%.

According to the scanning angle distance, the acquisition time function of continuous raster scanning can be obtained as follows:

$$t = t_h + t_v = \frac{(\theta_{uh} - 2\theta_h)\cdot\theta_{uv}}{2(1-K)\theta^2 F_h} + \frac{\theta_{uv} - 2\theta_v}{2(1-K)\theta F_v}. \tag{3}$$

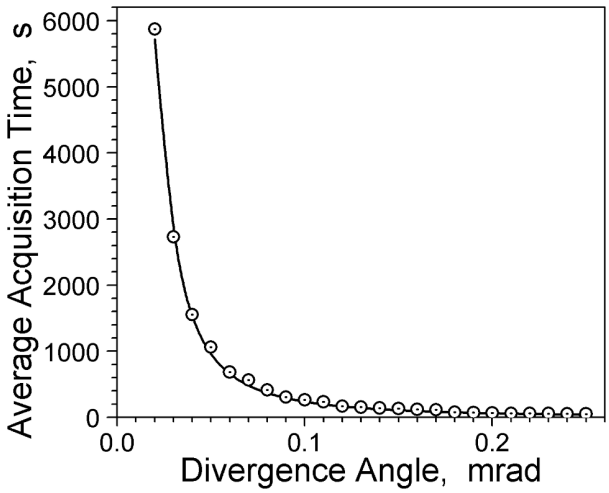

Fig. 3. The theoretical calculation of the average acquisition time (solid curve) and the Monte Carlo simulation curve (dots).

Combined with Eqs. (1) and (3), the average acquisition time can be determined as

$$T = \int_{-\theta_{uh}/2}^{\theta_{uh}/2}\int_{-\theta_{uv}/2}^{\theta_{uv}/2}(t_h + t_v) f(\theta_v, \theta_h)\, d\theta_v\, d\theta_h. \tag{4}$$

Assuming that the elevation and horizontal errors are independent of each other, the standard deviation σ_v and σ_h are 0.6 mrad and 1.8 mrad, respectively, the scanning range is taken as $\theta_{uh} = 6\sigma_h$ and $\theta_{uv} = 6\sigma_v$, the scanning overlap factor $K = 15\%$, the frame frequency of the CCD camera $F_h = 10$ Hz, and the control bandwidth of capture system $F_v = 10$ Hz. According to Eq. (4), the relationship curve between the divergence angle and average acquisition time is obtained, and the acquisition time is simulated 2000 times by the Monte Carlo method. The theoretical values are compared with the simulation data in Fig. 3.

In Fig. 3, we see that the theoretical derivation is basically consistent with the simulation value, thus verifying the correctness of the theoretical formula. Within the range of the beam divergence angle $\theta < 100$ μrad, the average acquisition time decreases significantly with increase in θ, and then the change of average acquisition time tends to be smooth. The simulation results show that the acquisition time can be significantly reduced by increasing the beam divergence angle under a certain acquisition probability.

3.2. Receiving Power Affected by Atmospheric Transmission and Pointing Errors

Under the influence of atmospheric transmission and pointing errors, it is necessary to analyze the average receiving power for the signal light to maximize the compression of collimated beams to achieve the minimum transmitting power. The pointing error is the angular deviation between the actual beam emitted by the transmitter and the beam positively aligned. The pointing accuracy is defined as three times the standard deviation σ of the pointing error, and the probability of the pointing error being less than 3σ is 99.73% [12, 13]. The transmission and reception schematic diagram with pointing deviation is shown in Fig. 4, where A is the transmitter and B is the receiver. Cartesian coordinate systems are

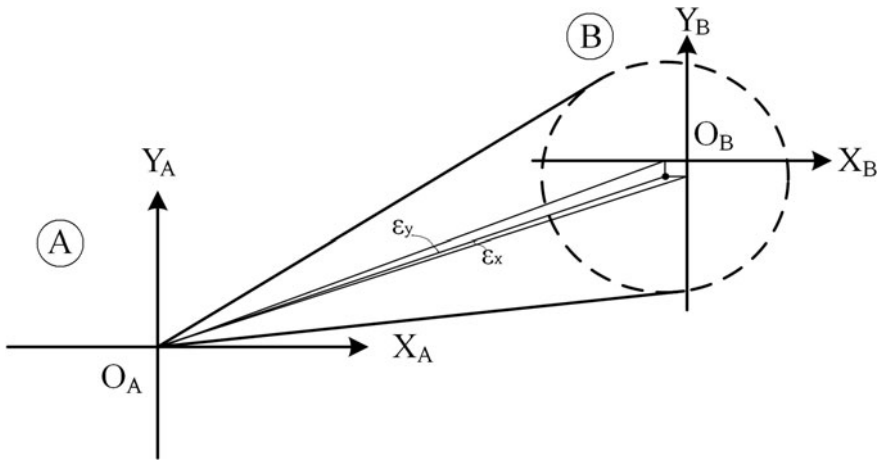

Fig. 4. Schematic diagram of transmission and reception.

established with the transmitting antenna and the plane center O_A and O_B of the receiving antenna. The angle deviations of the elevation and horizontal directions are ε_x and ε_y, respectively.

Using a narrow line-width laser as a carrier, the signal light is generally a fundamental mode Gauss beam. Assuming that the transmitting power is P_t, the amplitude distribution in the cross section perpendicular to the propagation direction at the source plane can be expressed as

$$U(r,0) = \left(\theta\sqrt{2P_t\pi}/2\lambda\right) \cdot \exp\left[-\pi^2\theta^2\boldsymbol{r}^2/4\lambda^2\right], \tag{5}$$

where $\boldsymbol{r} = (x, y)$ is a vector in the cross section perpendicular to the propagation direction, and λ is the wavelength of the signal light.

Based on the generalized Huygens–Fresnel principle [14], we calculate the average intensity of fundamental mode Gauss beams propagating through turbulent atmosphere; it is

$$\langle I(\boldsymbol{r}, z)\rangle = \left(\pi P_t/2A\lambda^2 z^2\right) \cdot \exp(-k^2\boldsymbol{r}^2/4z^2A). \tag{6}$$

Here,

$$A = \frac{2}{\theta^2 z^2} + \frac{\theta^2\pi^2}{8\lambda^2} + \pi^2 k^2 z \int_0^1 \int_0^\infty \Phi_n(\varkappa)\xi^2\varkappa^3\, d\varkappa\, d\xi, \tag{7}$$

$\Phi_n(\varkappa)$ is the spatial power spectrum of the turbulence refractive-index fluctuations, with the Hill spectral model used,

$$\Phi_n(\varkappa) = 0.033\, C_n^2 \left[1 + a_1(\varkappa/\varkappa_l) - a_2(\varkappa/\varkappa_l)^{7/6}\right] \frac{\exp(-\varkappa^2/\varkappa_m^2)}{(\varkappa^2 + \varkappa_0^2)^{-11/6}}, \qquad 0 \le \varkappa \le \infty, \tag{8}$$

and C_n^2 is the structure constant of atmospheric refractive index, with $\alpha_1 = 1.802$, $\alpha_2 = 0.254$, $\varkappa_l = 3.3/l_0$, $\varkappa_m = 5.92/l_0$, and $\varkappa_0 = 2\pi/L_0$; l_0 and L_0 represent the internal and external scales of turbulence.

Considering that the laser propagation in the atmosphere is also affected by the attenuation effect, the average intensity distribution at z can be obtained by Eq. (6); it is

$$\langle I(\boldsymbol{r}, z)\rangle = \frac{\pi P_t}{2A\lambda^2 z^2} \exp\left(-k^2\boldsymbol{r}^2/4z^2A\right) \exp\left[-\sigma(\lambda)z\right]. \tag{9}$$

Here, $\sigma(\lambda)$ is the attenuation coefficient, which can be expressed as

$$\sigma(\lambda) = \frac{3.91}{V}\left(\frac{\lambda}{550}\right)^{-q}, \tag{10}$$

with V being the visibility and q the size distribution of scattered particles.

Considering the existence of pointing errors, the received signal strength is affected by the tracking and aiming deviation [15, 16]. In view of Eq. (9), we can obtain the power received by the receiving antenna with radius D in the presence of pointing error; it is

$$p_r(z) = \iint\limits_{A_r} \langle I(r,z)\rangle\, dS = \int_{-D}^{D}\int_{-\sqrt{D^2-y^2}}^{\sqrt{D^2-x^2}} \frac{\pi P_t}{2\lambda^2 z^2 A}\, \exp\left[-\frac{k^2((x-x')^2+(y-y')^2)}{4z^2A} - \sigma(\lambda)z\right] dx\, dy, \tag{11}$$

where $x' = 2z\tan(\varepsilon_x/2)$ and $y' = 2z\tan(\varepsilon_y/2)$ are the displacement components of the horizontal and elevation deviations on the X and Y axes, respectively.

Without special explanation, the transmitting optical power $P_t = 600$ mW, wavelength $\lambda = 1550$ nm, link distance $z = 10$ km, turbulence internal and external scales $l_0 = 0.01$ m and $L_0 = 10$ m, atmospheric refractive-index structure constant $C_n^2 = 1.7 \cdot 10^{-14}$, visibility $v = 10$ km, receiving antenna aperture $D = 10$ cm, and pointing accuracy $\sigma = 17$ μrad. The relation curve between the received power and the divergence angle under the influence of the signal light through the atmospheric transmission and the pointing errors can be obtained from Eq. (11), as shown in Fig. 5.

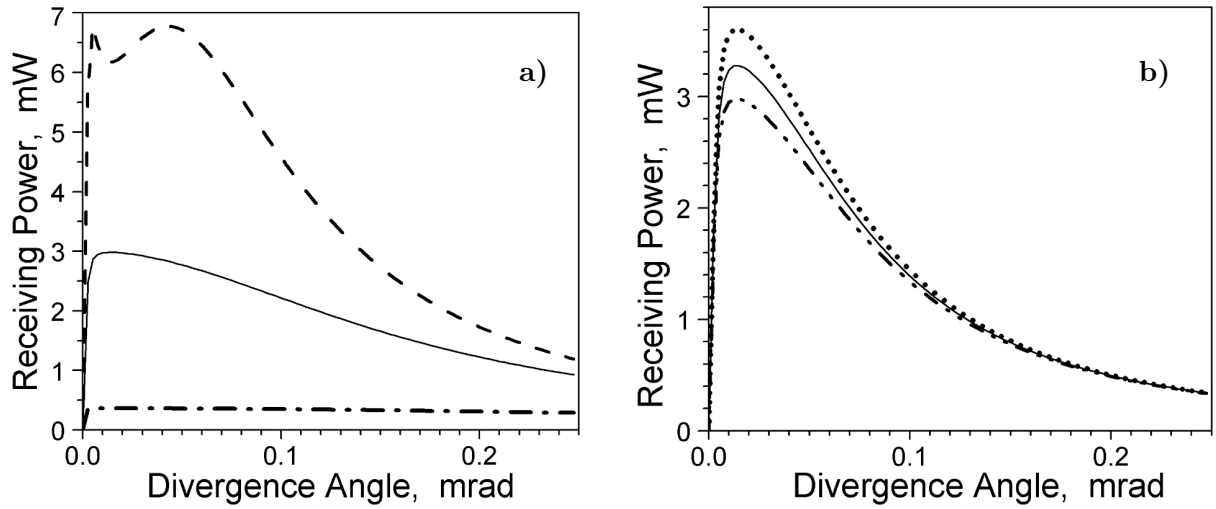

Fig. 5. Receiving power and divergence angle curve at different turbulence intensities (a), where $C_n^2 = 1.7 \cdot 10^{-13}$ (dash-dotted curve), $C_n^2 = 1.7 \cdot 10^{-14}$ (solid curve), and $C_n^2 = 1.7 \cdot 10^{-15}$ (dashed curve), along with different pointing errors (b), where $\varepsilon_x = \varepsilon_y = 5.5$ μrad (dotted curve), $\varepsilon_x = 10$ μrad and $\varepsilon_y = 5.5$ μrad (solid curve), and $\varepsilon_x = \varepsilon_y = 10$ μrad (dash–dot-dotted curve).

Figure 5 shows clearly that with increase in the beam divergence angle, the receiving power increases first and then decreases. Therefore, in the communication phase, minimal divergence angle is not necessarily the best option.

Figure 5 a illustrates the curve of the relationship between receiving power and divergence angle under different turbulence intensities. The turbulence on the signal light influences not only the attenuation of

the optical power but also the spreading of the beam. Therefore, with the enhancement of turbulence, the more obvious the beam spreading effect, the lower the receiving power, and the smaller the optimum divergence angle.

Figure 5 b illustrates the curve of the relationship between receiving power and the divergence angle under different pointing errors. We can see that the receiving power increases with decrease in the pointing errors. The optimum divergence angle is related to the minimum pointing errors on the elevation and horizontal. The smaller the pointing errors, the smaller the optimum divergence angle, and the narrower the optimum range. The simulation results show that for 10 km communication links, the maximum receiving power is obtained when the divergence angle is around 30 μrad, with the pointing accuracy of 17 μrad and different turbulence intensities.

3.3. Principle of Automatic Focusing Control

The principle of automatic focusing control is to drive a stepping motor to change the distance between the transmitting antenna objective lens and the eyepiece before the acquisition starts, so as to increase the defocus, thereby increasing the divergence angle and improving the acquisition efficiency. After the acquisition, image processing is performed on the spot captured by the receiver. The size information of the spot is used as a feedback. When the radius of the spot is larger than the set threshold, the driving stepper motor adjusts the focal length of the transmitting antenna to reduce the defocus and divergence angle.

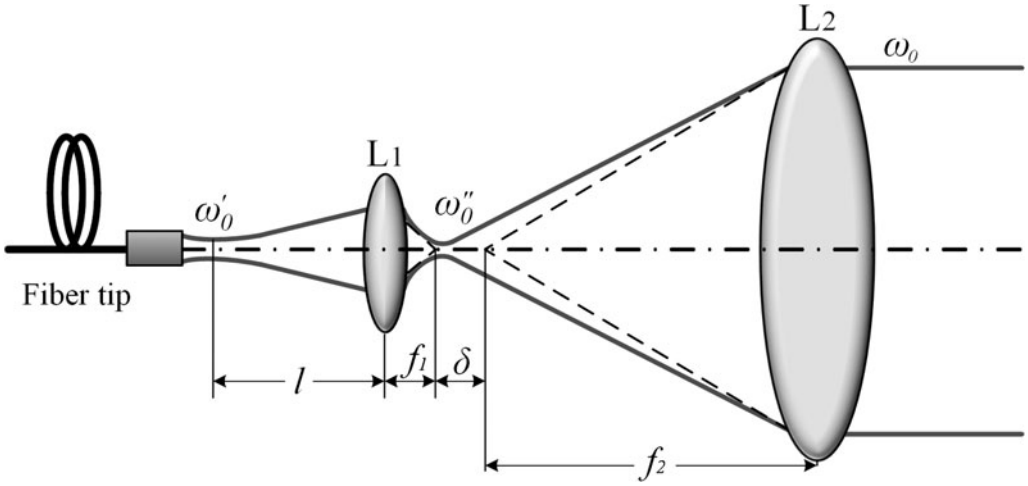

Fig. 6. Schematic diagram of automatic focusing control.

The schematic diagram is shown in Fig. 6. A light source with a beam waist radius of ω_0' is generated by the fiber tip. After transmission through the eyepiece L_1 with a focal length of f_1, a small diameter focusing point is formed on the rear focal plane of the L_1; the beam waist radius is ω_0''. When ω_0'' falls on the rear focal plane of L_2, the optical interval is 0, and a good collimation effect can be obtained. By changing the distance between the lens L_1 and L_2 and the defocusing amount δ, the divergence angle of the collimated beam is changed.

According to the *ABCD* formula, when the q parameter is transformed through the optical system,

the divergence angle of the emitted beam can be expressed as follows:

$$\theta = \frac{2\lambda}{\pi}\sqrt{\frac{1}{M^2 w'^2(l)} + \frac{\delta^2\pi^2 w'^2(l)^2}{f_1'^2 f_2^2 \lambda}}\,, \tag{12}$$

where $M = f_2/f_1'$ is the collimation ratio, f_1' is the distance between the optical waist and the lens L_1, $\omega'(l)$ is the radius of the Gauss beam at l, and f_1' and $\omega'(l)$, respectively, are

$$\omega'(l) = \omega_0'\sqrt{1 + \left(\lambda l/\pi\omega_0'^2\right)^2}, \qquad f_1' = f_1 + \frac{(l-f_1)f_1^2}{(l-f_1)^2 + \left(\pi\omega_0'^2/\lambda\right)^2}. \tag{13}$$

It can be seen from Eq. (12) that the divergence angle of the collimated beam is affected by the collimation ratio and l, and the relationship between the divergence angle and defocus is not linear. In order to quantitatively analyze the effect of defocusing on the divergence angle of a collimated beam and provide a reference for system design, numerical calculation is carried out. The parameters $\omega_0' = 5$ μm, $f_1 = 2$ cm, and $f_2 = 38$ cm were taken. The relationship between defocus and the beam divergence angle is shown in Fig. 7.

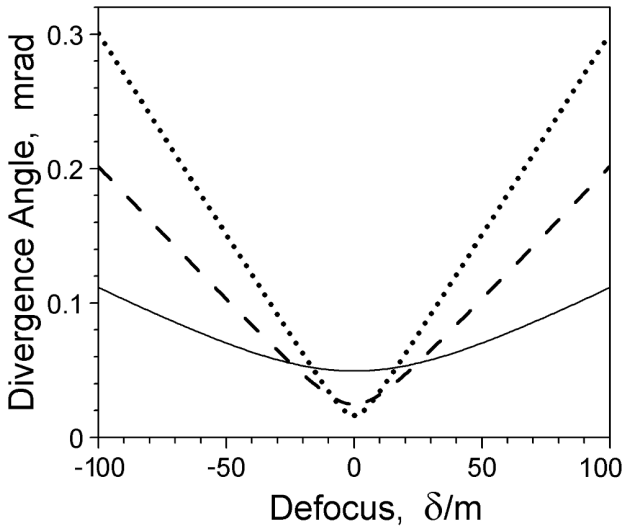

Fig. 7. Curves of relationship between defocus and beam divergence angle, where $l = 0.04$ (solid curve), $l = 0.08$ (dashed curve), and $l = 0.12$ (dotted curve).

As can be seen from Fig. 7, ω_0'' falls on the rear focus plane of objective lens L_2, the defocus is 0, and the divergence angle of collimated beam is the smallest. The $\delta > 0$ is a positive defocus, indicating that ω_0'' falls before the rear focus plane of L_2. The $\delta < 0$ is a negative defocus, indicating that ω_0'' falls behind the rear focus plane of L_2. The larger the $|\delta|$, the larger the divergence angle of the collimated beam. When defocusing is adjusted, the divergence angle of the collimated beam changes gradually. In the same defocusing range, the larger l, the larger the adjustment range of the collimating beam, and the smaller the minimum divergence angle. According to the simulation results, different divergence angles can be obtained by choosing the defocusing amount and l reasonably.

4. Experimental Result

A 10 km coherent optical communication link with 1550 nm wavelength and 600 mW transmit power was successfully established using an automatic focusing APT system. The acquisition time is less than 60 s when the beam divergence angle in acquisition phase is 1 mrad. The spot image detected by the CCD camera at the receiver using the automatic focusing control method is shown in Fig. 8. In Fig. 8 a, we show the image of the spot detected by the CCD camera at the receiver after the light beam in the acquisition phase is transmitted through the atmosphere. After the image processing, the radius is 64.94 cm; see Fig. 8 c. In Fig. 8 b, we show the spot image after the signal light is captured, and

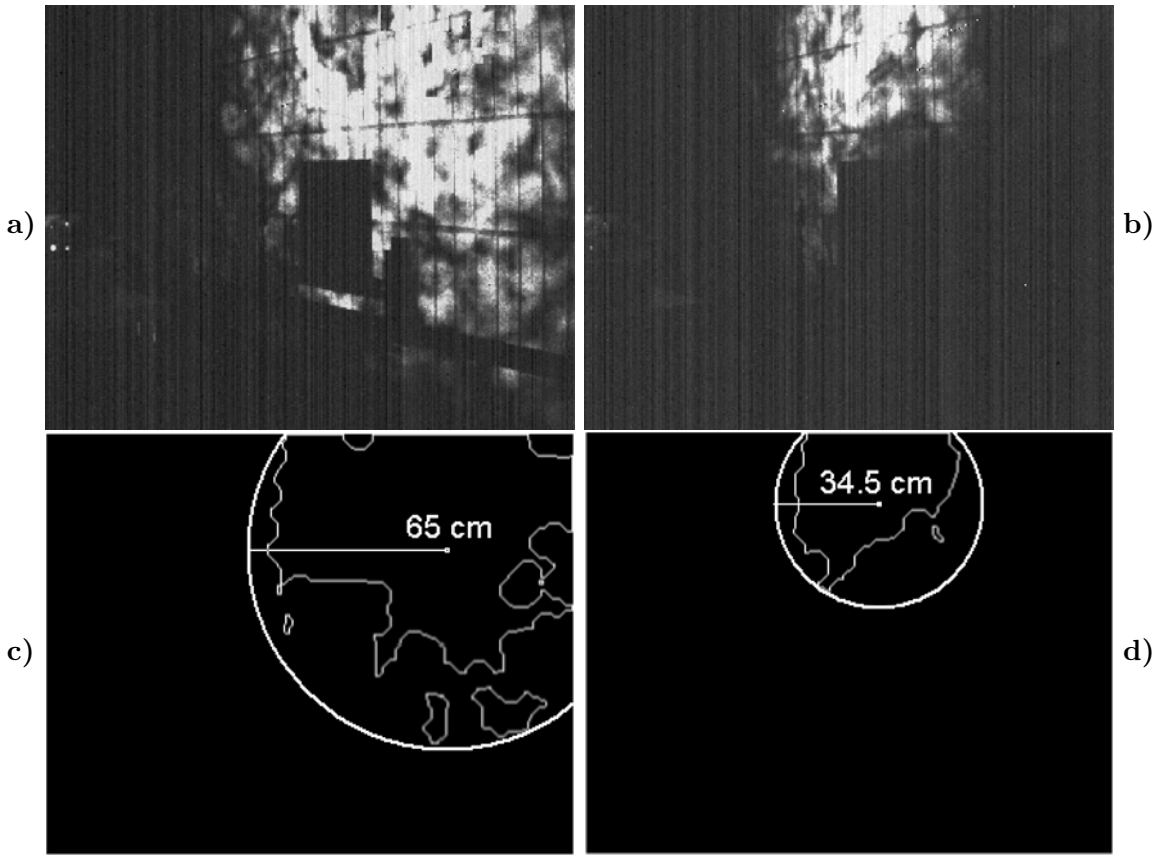

Fig. 8. Receiver spot image; here, the spot image in acquisition phase (a) and in communication phase (b) along with the spot radius at capture stage (c) and at communication stage (d).

the divergence is adjusted to change the divergence angle. After the image processing, the radius was detected to be 34.50 cm; see Fig. 8 d.

When communicating with the beam in the capture phase, the power of the receiving end coupled into the single-mode fiber is less than – 50 dBm at the same transmitting power. So, after the capture phase is completed, the stepper motor is driven to focus control. In Fig. 9, we show the power of the receiving end coupled into a single-mode optical fiber in three weather conditions of rain, fog, and sunshine, when the divergence angle of the signal light after focusing control is close to 30 μrad, which meets the actual communication requirements in various environments.

In Fig. 9 a, the average power of the coupled fibers is – 38.21 dBm with a standard deviation of – 41.58 dBm. In Fig. 9 b, the average power is – 40.76 dBm with a standard deviation of – 43.01 dBm. In Fig. 9 c, the average power is – 22.29 dBm with a standard deviation of – 23.71 dBm.

It can be seen from the average receiving power that the average receiving power in sunny days is much better than that in rainy and foggy days, because the visibility in sunny days is much larger than that in rainy and foggy days, and it is less affected by the atmospheric attenuation effect. The fluctuation trend of the receiving light power is that its range in sunny days is larger than that in rainy and foggy days, and the fluctuation of the receiving light power in rainy days is the smallest. The main reason is that the surface temperature is low, and the temperature difference is small in rainy days. At the

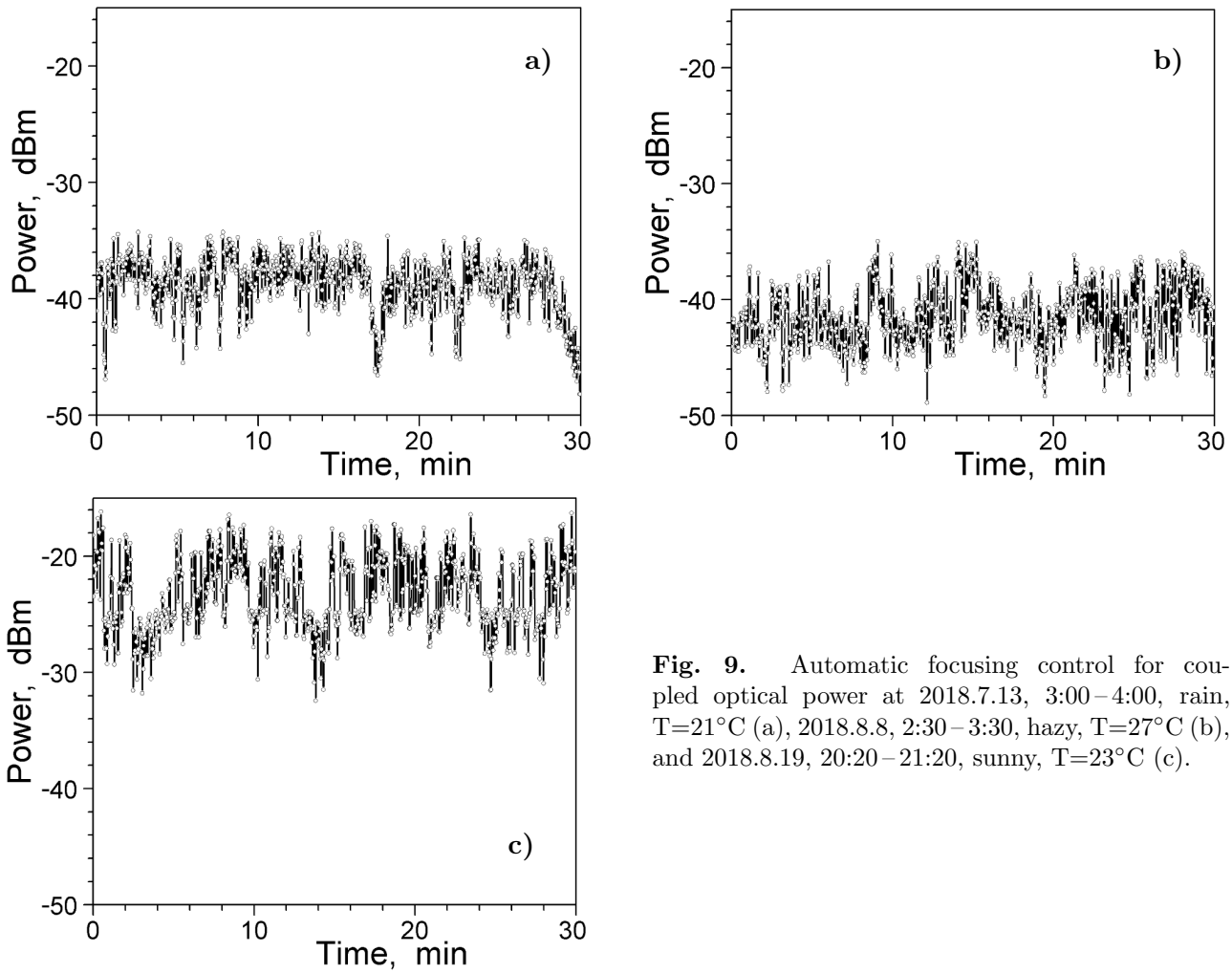

Fig. 9. Automatic focusing control for coupled optical power at 2018.7.13, 3:00 – 4:00, rain, T=21°C (a), 2018.8.8, 2:30 – 3:30, hazy, T=27°C (b), and 2018.8.19, 20:20 – 21:20, sunny, T=23°C (c).

same time, rainfall reduces the nonuniform components in the air, which makes the fluctuation of light intensity caused by atmospheric turbulence less affected.

5. Summary

In this paper, we proposed an automatic focusing method to optimize the beaconless APT system to solve the requirement contradiction of the divergence angles between the communication phase and the acquisition phase. We derived the expression of capture time, analyzed the receiving power affected by atmospheric transmission and tracking error, and obtained the relationship between defocusing and divergence angle of the collimated beam. The feasibility of the automatic focusing APT system is verified by experiments. The experimental results show that when the divergence angle is 0.1 mrad, the average acquisition time is less than 60 s, the receiver spot radius is 64.94 cm, and the coupling optical power is less than – 50 dBm. After automatic focusing control, the beam with divergence angle of 0.03 mrad is used to communicate, the receiver spot radius is 34.50 cm, and the coupling optical power under different weather increased from – 43 dBm to – 23 dBm. We effectively solved the requirement contradiction of

the divergence angles between communication phase and signal light acquisition phase and improved the acquisition efficiency and communication system performance.

Acknowledgments

The authors acknowledge the financial support provided within the Key Industry Innovation Chain Project of Shaanxi Province No. 2017ZDCXL-GY-06-01, the Scientific Research Project of Shaanxi Provincial Department of Education No:18jk0341, and the Xi'an Science and Technology Innovation Guidance Project No. 201805030yd8cg14 (12).

References

1. T. T. Nielsen, *Proc. SPIE*, **2381**, 194 (1995).
2. X. Ma, L. Liu, X. Zhang, and J. Tang, *Appl. Opt.*, **49**, 718 (2010).
3. B. Tu, L. Liu, Y. Liu, et al., *Appl. Opt.*, **52**, 3147 (2013).
4. K. J. Held, and J. D. Barry, *Opt. Eng.*, 27, 325 (1988).
5. S. Bai, J. Qiang, L. Zhang, and J. Wang, *Opt. Lett.*, **40**, 3750 (2015).
6. J. Wang, J. M. Kahn, and K. Y. Lau, *Appl. Opt.*, **41**, 7592 (2002).
7. X. Li, S. Yu, J. Ma, and L. Tan, *Opt. Express*, **19**, 2381 (2011).
8. D. He, Q. Wang, B. Qi, et al., *Appl. Opt.*, **57**, 1351 (2018).
9. T. T. Nguyen, K. M. Riesing, R. W. Kingsbury, and K. Cahoy, *Proc. SPIE*, **9354**, 93540O (2015).
10. B. Smutny, R. Lange, H. Kämpfner, and K. Cahoy, *Proc. SPIE*, **6877**, 687702 (2008).
11. X. Li, S. Yu, J. Ma, et al., *J. Russ. Laser Res.*, **33**, 143 (2012).
12. T. Tolker-Nielsen and G. Oppenhauser, *Proc. SPIE*, **4635**, 1 (2002).
13. J. W. Alexander, S. Lee, and C. Chen, *Proc. SPIE*, **3615**, 230 (1999).
14. J. C. Ricklin and F. M. Davidson, *J. Opt. Soc. Am. A*, **19**, 1794 (2002).
15. J. Wang, J. Lv, G. Zhang, and G. Wang, *Opt. Express*, **23**, 20655 (2015).
16. V. V. Mai and H. Kim, *IEEE Photon. J.*, **11**, 1 (2019).